International Journal of Nanomedicine

Dovepress
Taylor & Francis Group

Open Access Full Text Article

ORIGINAL RESEARCH

Comparative Evaluation of Three Nanoparticle Vaccines Targeting the Prefusion F Protein of Respiratory Syncytial Virus: Immunogenicity and Protective Efficacy

Jie Jiang, Hongqiao Hu, Lei Cao, Naiying Mao, Zhen Zhu, Na Wang, Yuqing Shi, Hai Li, Yan Zhang

National Key Laboratory of Intelligent Tracking and Forecasting for Infectious Diseases, NHC Key Laboratory of Medical Virology and Viral Disease, National Institute for Viral Disease Control and Prevention, Chinese Center for Disease Control and Prevention, Beijing, 102206, People's Republic of China

Correspondence: Yan Zhang; Hai Li, Email zhangyan@ivdc.chinacdc.cn; lihai@ivdc.chinacdc.cn

Purpose: To evaluate the immunogenic potential of three different nanoparticle (NP) platforms for respiratory syncytial virus (RSV) prefusion (pre-F) protein vaccines.

Methods: Three NP platforms—24-mer ferritin (Fe), 60-mer lumazine synthase (LuS), and 120-subunit I53-50—were engineered to display RSV pre-F trimers (DS2) via SpyTag-SpyCatcher (ST-SC) conjugation (DS2-Fe, DS2-LuS) or direct genetic fusion (DS2-I53-50). The assembled particles were characterized using size-exclusion chromatography (SEC), SDS-PAGE, electron microscopy (EM), and dynamic light scattering (DLS). Antigenicity was evaluated using enzyme-linked immunosorbent assay (ELISA) and surface plasmon resonance (SPR) with prefusion-specific neutralizing antibodies. Immunogenicity and protective efficacy were evaluated in BALB/c mice following a prime-boost immunization, with analyses of humoral and cellular immune responses as well as post-challenge protection.

Results: All three NP platforms successfully displayed the DS2 antigen while preserving its prefusion conformation. Notably, DS2-I53-50 demonstrated superior assembly quality and particle homogeneity relative to DS2-Fe and DS2-LuS. Compared to soluble DS2, all three DS2-NPs exhibited enhanced binding affinity (7- to 12-fold increase) to prefusion-specific antibodies (D25, AM14). In vivo, all DS2-NPs elicited higher levels of RSV-specific neutralizing antibodies and induced a more balanced Th1/Th2 immune response, with DS2-I53-50 generating significantly greater neutralizing antibody titers (1.7- to 2.4-fold increase) against both prototype RSV strains (LONG, 18537) and circulating genotypes (ON1, BA9). Immune cell profiling further revealed that all three DS2-NPs enhanced germinal center formation, facilitated follicular dendritic cell recruitment, and expanded memory T cell populations. Following RSV challenge, all DS2-NPs vaccines conferred significant protection, evidenced by accelerated weight recovery, reduced lung viral loads, and mitigated pulmonary pathology. Among them, DS2-I53-50 provided the most robust protection, achieving a 3.7-log reduction in viral titers and minimal lung pathology.

Conclusion: NP platforms significantly enhanced the immunogenicity of RSV DS2 antigens, with DS2-I53-50 eliciting the strongest immune responses and protective efficacy. These findings underscore the potential of rationally designed NP-based vaccines for RSV.

Keywords: respiratory syncytial virus, RSV, nanoparticle vaccine, ferritin, lumazine synthase, I53-50, prefusion F protein, immunogenicity, protective efficacy

Introduction

Respiratory syncytial virus (RSV) is a major global cause of acute lower respiratory tract infections (ALRTIs), disproportionately affecting infants, older adults, and immunocompromised populations.[1,2] For decades, the absence of a licensed RSV vaccine has exacerbated this public health crisis. A pivotal shift occurred in 2023 when the US FDA approved two subunit RSV vaccines—Arexvy (GSK), Abrysvo (Pfizer), the latter also authorized for maternal

Received: 14 April 2025
Accepted: 8 July 2025
Published: 15 August 2025

Graphical Abstract

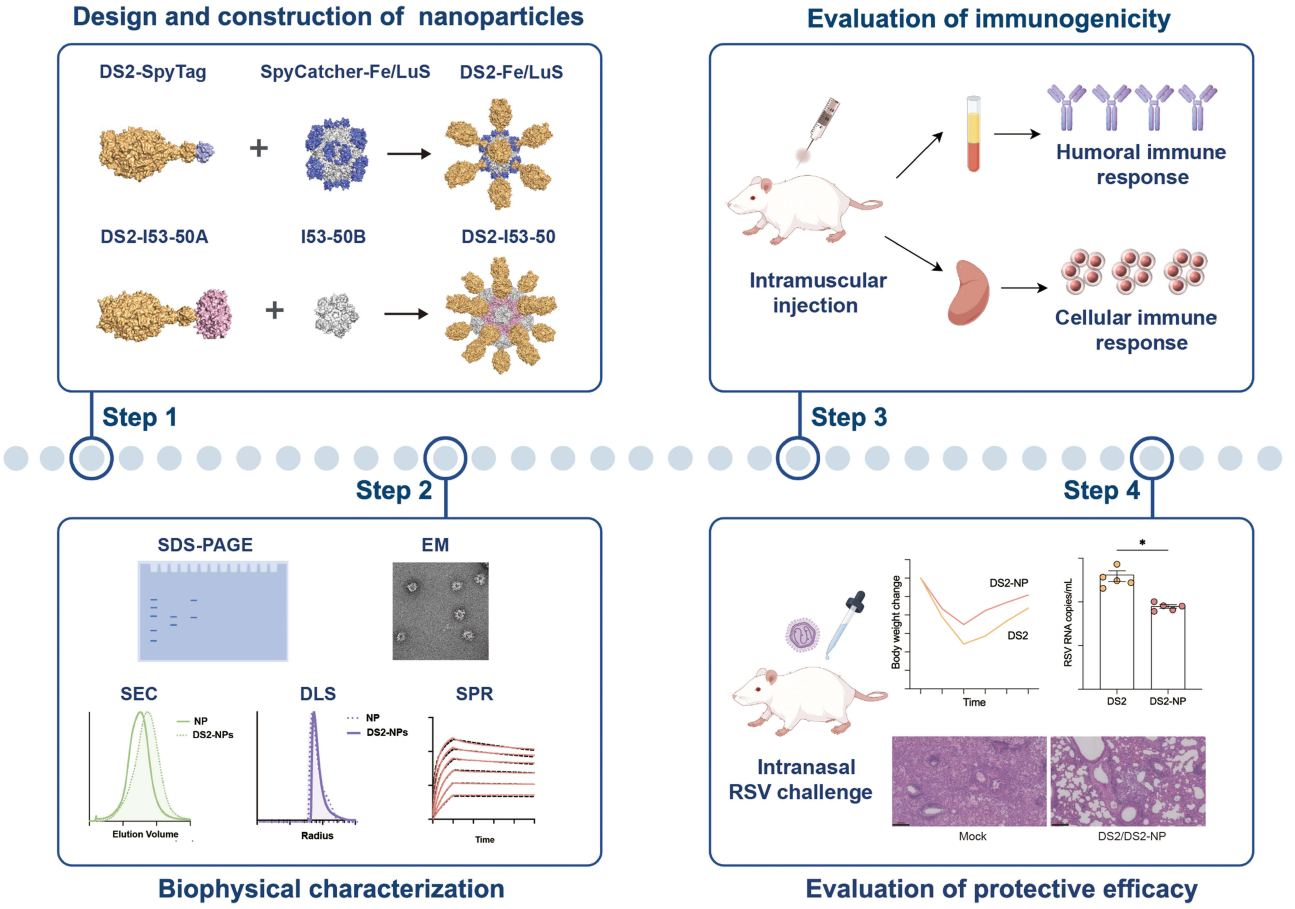

immunization to protect infants.[2] In 2024, Moderna's mRNA-1345 vaccine received approval for older adults,[3] further advancing the field of RSV vaccine development.[4]

Current RSV vaccines primarily target the prefusion (pre-F) conformation of the RSV fusion (F) glycoprotein, which contains critical neutralizing epitopes recognized by potent antibodies such as D25 and AM14.[5,6] However, the metastable nature of pre-F, which readily transitions into a less immunogenic post-F form, has historically hindered vaccine development.[2] Over the past decade, structural insights have enabled rational engineering to introduce stabilizing mutations that "lock" the pre-F trimer in its antigenically optimal conformation. Stabilization strategies include disulfide bond-based designs (eg, DS-Cav1, DS2),[7,8] stem–transmembrane fusion constructs (SC-TM),[9] and dynamic coupling-based regulation system such as TriM-5.[10] These engineering approaches significantly improve both the immunogenicity and in vivo stability of pre-F proteins, and have led to the incorporation of stabilized constructs like DS-Cav1 and DS2 in several licensed RSV vaccines.[10]

Despite these advances, soluble stabilized pre-F proteins often elicit suboptimal immunogenicity and limited durability when administered as traditional subunit vaccines.[2,4] Nanoparticle (NP) vaccine platforms have emerged as promising strategies by mimicking the repetitive geometry of viral surfaces to enhance B cell receptor (BCR) crosslinking, stimulating robust germinal center (GC) responses, and promoting durable humoral immunity.[11–13] Among these platforms, ferritin (Fe), lumazine synthase (LuS), and the computationally designed I53-50 represent protein-based NP scaffolds with distinct spatial architectures, particle diameters, and assembly mechanisms. Fe self-assembles into octahedral 24-mers, LuS forms icosahedral 60-mers,[14] and I53-50 generates icosahedral 120-subunit structures through co-assembly of trimeric I53-50A and pentameric I53-50B components.[15]

These platforms have demonstrated promising immunogenicity against a range of pathogens, including influenza,[16] HIV,[17] SARS-CoV-2,[18] RSV,[19] and Epstein–Barr virus (EBV).[20] For antigen display, Fe and LuS platforms commonly use the SpyTag–SpyCatcher (ST-SC) covalent ligation system to achieve stable, site-specific conjugation,[21] which has been shown to elicit potent immune responses in prior studies.[18,22,23] In contrast, the I53-50 platform allows direct genetic fusion of antigens to 20 symmetric sites on its trimeric I53-50A component.[15] Marcandalli et al (Cell, 2019) demonstrated this approach by genetically displaying stabilized RSV pre-F (DS-Cav1) on I53-50 NPs, resulting in significantly enhanced neutralizing antibody responses.[19]

Despite these advances, comparative studies evaluating the immunogenicity of different NP platforms presenting the same stabilized RSV pre-F antigen remain limited. In this study, we generated three NP-based RSV vaccines using the DS2 stabilized pre-F construct: DS2-Fe and DS2-LuS via ST-SC conjugation, and DS2-I53-50 via genetic fusion. All three NP formulations exhibited efficient assembly and conjugation of DS2 trimers, with increased antigen–antibody binding affinity relative to soluble DS2. In vivo immunization studies in BALB/c mice revealed that, despite differences in particle geometry and assembly strategies, all three NP vaccines elicited potent humoral and cellular immune responses and conferred robust protection against both prototype and circulating RSV strains. These results provide valuable insights into how NP scaffolds enhance antigen immunogenicity and support the rational development of next-generation NP-based RSV vaccines.

Material and Methods

Cells and Virus

HEK293F cells (Life Technologies, Carlsbad, CA) were cultured in serum-free Expi293™ Expression Medium (Thermo Fisher Scientific, Waltham, MA) under suspension conditions (37°C, 5% CO_2, 125 rpm shaking). HEp-2 cells (ATCC CCL-23) were cultured in Dulbecco's Modified Eagle Medium (DMEM; HyClone, South Logan, UT) supplemented with 10% fetal bovine serum (FBS; Gibco, Grand Island, NY), 1% penicillin-streptomycin (HyClone), and 1% HEPES (HyClone) at 37°C in a 5% CO_2 atmosphere. For viral studies, prototype strains of RSV including subtype A (LONG strain; ATCC VR-26) and subtype B (18537 strain; ATCC VR-1580), along with circulating strains (ON1 genotype 6049, isolated 2019; BA9 genotype R5, isolated 2023) provided by the Department of Measles of the Chinese Institute for Viral Disease Control and Prevention. These strains were propagated in HEp-2 cells and titrated via plaque assay for neutralization studies.

Animal Studies

Specific pathogen-free female BALB/c mice (aged 6–7 weeks) were procured from Beijing Vital River Laboratory Animal Technology Co., Ltd. The mice were housed under standardized conditions (12-hour light/dark cycle, 22°C, 50% humidity) with ad libitum access to autoclaved food and purified water to ensure optimal health and minimize experimental variables. All animal experiments were conducted in accordance with the *Guidelines for Ethical Review of Laboratory Animal Welfare of China* and were approved by the Ethics Committee of the Institute for Viral Disease Control and Prevention (approval no.: 20231113086).

Plasmid Design and Construction

The RSV F construct DS2 (PDB: 5K6H),[8] based on the RSV Long strain F protein, incorporates the following stabilizing mutations: S46G, E92D, A149C, S155C, S190F, V207L, S215P, S290C, L373R, S458C, and K465Q. The DS2 gene was cloned into the pcDNA3.4 vector, and subsequently codon-optimized and synthesized (Tsingke Biotechnology). The IgG heavy and light chain genes of D25 (target antigenic sites Ø of RSV pre-F), AM14 (target antigenic sites V of RSV pre-F), and palivizumab (present in both pre-F and post-F) were cloned into the pcDNA3.4 vector. DS2 was fused to SpyTag (ST; N-terminal 16 residues) or I53-50A NP components[15] and cloned into pcDNA3.4. SpyCatcher-ferritin (SC-Fe), SpyCatcher-lumazine synthase (SC-LuS), and I53-50A/B subunits were synthesized and inserted into pET28a+ with a C-terminal His-tag. Amino acid sequences for all constructs are provided in Table S1.

Protein Expression and Purification in Mammalian Cells

Expi293F cells (3×10^6 cells/mL) were transiently transfected with plasmids encoding DS2, ST-DS2, or DS2-I53-50A using the Expifectamine 293 Transfection Kit (Thermo Fisher Scientific). Culture supernatants were harvested on day 5 and purified via nickel-nitrilotriacetic acid (Ni-NTA) immobilized metal affinity chromatography (wash buffer: 25 mM Tris-HCl pH 7.5, 300 mM NaCl, 60 mM imidazole; elution buffer: 25 mM Tris-HCl pH 7.5, 300 mM NaCl, and 300 mM imidazole), followed by size exclusion chromatography (SEC) on a Superose 200 Increase 10/300 GL column (GE Healthcare, Chicago, IL) in PBS. Monoclonal antibodies (D25, AM14, and palivizumab) were similarly produced and purified using a HiTrap MabSelect PrismA column (GE Healthcare), washed with 20 mM sodium phosphate and 150 mM sodium chloride buffer (pH 7.4), and eluted with 100 mM $Na_3C_6H_5O_7$ sodium citrate (pH 3.0) into a 1/2 volume of PBS.

Protein Expression and Purification in Bacterial System

Plasmids encoding SC-Fe, SC-LuS, I53-50A, and I53-50B were transformed into BL21 (DE3) cells (TIANGEN Biotech, Beijing, China). Single colonies were cultured in lysogeny broth (LB) medium with 50 μg/mL kanamycin at 37°C overnight. Seed cultures were transferred to 1 L of LB medium with kanamycin and grown to an OD_{600} of 0.6–0.8. Protein expression was induced with 0.5 mM isopropyl β-D-1-thiogalactopyranoside (IPTG) at 16°C for 16–20 h. Bacterial pellets were lysed via sonication in lysis buffer (50 mM Tris-HCl pH 8.0, 300 mM NaCl, 30 mM imidazole, 0.75% CHAPS, 1 mM PMSF), and target proteins were purified using Ni-NTA chromatography (elution buffer: 50 mM Tris-HCl pH 8.0, 300 mM NaCl, 300 mM imidazole, 0.75% CHAPS). The eluted protein was further purified using SEC (Superdex 200 Increase 10/300 GL) and analyzed via sodium dodecyl-sulfate polyacrylamide gel electrophoresis (SDS-PAGE). Endotoxin levels were reduced using the ToxinEraser Endotoxin Removal Kit (GenScript Biotech, Nanjing, China) and confirmed to be <0.1 EU/mL.

DS2-Conjugated NP Assembly

DS2-Fe and DS2-LuS NPs were assembled by incubating SC-Fe or SC-LuS with a 2-fold molar excess of DS2-ST in PBS with 5% glycerol at 4°C for 16 h. DS2-I53-50 or I53-50 NPs were formed by mixing DS2-I53-50A or I53-50A with I53-50B at a 1:1 molar ratio in PBS with 5% glycerol at 25°C for 3 h. Assembled NPs were purified via SEC (Superdex 200 Increase 10/300 GL) and validated using SDS-PAGE.

SDS-PAGE Analysis

The protein samples were combined with 5X sample buffer containing DTT, heated at 95°C for 5 min, and separated on 4–20% polyacrylamide gels (GenScript). Gels were immersed in Coomassie Brilliant Blue dye (Sangon Biotech, Shanghai, China) and analyzed using a ChemiDoc Imaging System (Bio-Rad).

Negative-Stain Electron Microscopy (EM)

Samples were diluted to 0.05 mg/mL in PBS, applied to glow-discharged grids, and stained with 2% uranyl acetate. The copper grid underwent a rapid cleaning procedure involving three sequential applications of ultrapure water, followed by three treatments with 0.2% (w/v) uranyl acetate solution. During the final staining step, the grid remained immersed in the uranyl acetate solution for 45s before being carefully blotted dry using filter paper. Images were acquired on a Talos L120C microscope (Thermo Fisher Scientific) at 120 kV and recorded at 57,000×.

Dynamic Light Scattering (DLS)

Protein samples (0.5 mg/mL in PBS) were pre-filtered through a 0.22-μm membrane. The Zetasizer Nano ZS90 instrument (Malvern PANalytical, Malvern, UK) was employed to assess the hydrodynamic diameter and polydispersity index of the protein samples. All measurements were conducted in triplicate at a controlled temperature of 25°C. The experimental data were collected and processed utilizing the instrument's proprietary software (Malvern).

Enzyme-Linked Immunosorbent Assay (ELISA)

Purified DS2 or DS2-conjugated NPs were coated onto 96-well microplates (Yingke Biotech, Haimen, China) by overnight incubation at 4°C (100 μL/well, n = 3). Following immobilization, the plates were washed four times with PBS containing 0.05% Tween 20 (PBST). Non-specific binding sites were subsequently blocked through incubation with 5% bovine serum albumin (BSA) in PBS at 37°C for 2 h. Primary antibody incubation was performed using serially diluted D25 or AM14 antibodies (initial concentration: 50 μg/mL, five-fold dilution series in 2% BSA) at 37°C for 60 min. After washing, HRP-conjugated goat anti-human IgG antibody (ZSGB-BIO, Beijing, China) at 1:5,000 dilution was added and incubated for 30 min at 37°C. Tetramethylbenzidine (TMB; Sangon Biotech) was added to initiate the chromogenic reaction. The reaction was terminated after 5 min by adding 50 μL of 2 M H_2SO_4, and absorbance was measured at 450 nm using a microplate reader.

Surface Plasmon Resonance (SPR)

Antibody D25 or AM14 were immobilized onto Biacore Series S CM5 chips to ~100 response units. DS2-Fe, DS2-LuS, and DS2-I53-50 NPs were flowed over the chip at 30 μL/min for 200 s, followed by an 800 s dissociation phase. The starting concentration for each sample was 50 nM. Sensor chips were regenerated using 10 mM glycine-HCl (pH 2.5).

Immunization of BALB/c Mice

Female BALB/c mice (n = 5 per group) received intramuscular administration of either 5 μg DS2 or equimolar doses of DS2-Fe (8.44 μg), DS2-LuS (8.01 μg), and DS2-I53-50 (8.96 μg) NPs at days 0 and 21, with adjuvant of 50 μg aluminum hydroxide (Al; Croda, Snaith, UK) and 10 μg CpG oligonucleotides (type C; InvivoGen, San Diego, CA). Control groups received PBS (mock) or equivalent doses of NP formulations without antigen. Blood samples were collected at 35 d post-immunization, and mice were challenged intranasally with 6×10^5 plaque-forming units (PFUs) of RSV LONG strain virus at day 35. Body weights were monitored daily. Five days post-challenge, mice were humanely euthanized for tissue collection. Lung tissues were processed for both histopathological examination and quantitative viral load determination, while splenic tissues were harvested for single-cell suspension preparation and subsequent flow cytometric analysis of immune cell populations.

Serum ELISA

The 96-well microplate (Yingke Biotech) was coated overnight with DS2 antigen (1 μg/mL in PBS) at 4°C. Non-specific binding sites were subsequently blocked through incubation with 5% BSA in PBS at 37°C for 2 h. Serial five-fold dilutions of mouse serum samples (initial dilution 1:100 in 2% BSA/PBS) were applied to the antigen-coated wells and incubated at 37°C for 1 h. Following five washing cycles with PBST, HRP-conjugated goat anti-mouse IgG antibody (1:5,000 dilution; ZSGB-BIO) was added and incubated for 30 min at 37°C. For IgG isotype analysis, HRP-conjugated goat anti-mouse IgG1 (1:5,000; Abcam, Cambridge, UK) and IgG2a (1:20,000; Abcam) antibodies were used. Following the addition of TMB and quenching with 2 M H_2SO_4, absorbance was measured at 450 nm using the microplate reader. Data analysis was performed using GraphPad Prism 9, with reciprocal EC_{50} values calculated via four-parameter nonlinear regression.

RSV Virus Neutralization Assay

Mouse serum samples were subjected to heat inactivation at 56°C for 30 min to eliminate complement proteins. Serum was serially diluted four-fold, starting at 1:50 in DMEM with 2% FBS, and prepared in duplicate. Diluted serum was mixed in a 1:1 volume ratio with the RSV LONG, ON1,18537, and BA9 strains (1,000–1,500 PFUs/mL) and incubated at 37°C with 5% CO_2 for 2 h. The serum–virus complexes were then transferred to HEp-2 cells (3×10^5 cells/well) for 1 h to allow viral absorption. After removing the inoculum, cells were overlaid with 1.2% carboxymethylcellulose in maintenance medium and incubated for 48 h at 37°C. Post-incubation, the cell monolayer was fixed with 4% paraformaldehyde (PFA) and incubated with palivizumab followed by HRP-conjugated goat anti-human IgG (ZSGB-BIO). Viral plaques were quantified, and neutralizing antibody titers (IC_{50}) were determined through four-parameter nonlinear regression analysis using GraphPad Prism 9.

Splenocytes Isolation and Flow Cytometry

Spleens from immunized mice were harvested and processed using RPMI 1640 medium (Thermo Fisher Scientific). Single-cell suspensions were generated through mechanical dissociation followed by density gradient centrifugation using mouse lymphocyte separation medium (Dakewe Biotech Co., Ltd, Shenzhen, China). Splenocytes were stained with a fixable viability stain 780, and Fc receptor blocking was performed with anti-CD16/32 antibodies. For surface marker analysis, splenocytes were labeled with the following fluorochrome-conjugated antibodies in PBS containing 2% BSA: anti-CD45-APC-Cy7, anti-B220-FITC, anti-CD19-BV421, anti-CD3-PE-CF594, anti-CD4-FITC, anti-GL7-APC, anti-CD11b-PerCP-Cy5.5, anti-CD11c-PE-Cy7, anti-CD95-PE, anti-MHCII-Alexa Fluor 700, anti-F4/80-BV421, anti-PD-1-PE, anti-CD44-PE-Cy7, anti-CD62L-BV421, and anti-CXCR5-PercP-Cy5.5 (all antibodies from BD Biosciences, San Jose, CA, USA). For intracellular cytokine staining, cells were labeled with anti-CD3-PE-CF594, anti-CD4-FITC, anti-CD8-PE-Cy7, anti-IFN-γ-PE, anti-IL-2- PercP-Cy5.5, anti-IL-4-BV421, anti-TNF-α-APC, and isotype control anti-IgG1 antibodies. Fluorescence data acquisition was performed using a FACS Canto II flow cytometer (BD Biosciences), with subsequent analysis conducted on a BD LSRFortessa system. Compensation controls and fluorescence minus one control were included for proper gating strategy implementation and data interpretation.

Quantification of Viral Load in Lung Tissues

Lung tissues were aseptically collected and homogenized in PBS. A 200 μL aliquot of the homogenate was used for RNA extraction. The viral load of the RSV N gene was quantified using real-time quantitative reverse transcription PCR (qRT-PCR). Viral RNA copy numbers were determined by establishing a standard curve using a plasmid containing the RSV N gene, which allowed for the conversion of cycle threshold (Ct) values to corresponding RNA copy numbers. Viral RNA copy numbers were calculated as copies per milliliter (copies/mL) and expressed on a log10 scale. Each qRT-PCR run included positive controls and negative controls to ensure experimental reliability and accuracy.

Histopathological Evaluation and Lung Injury Scoring

Lung tissues were harvested immediately post-euthanasia and fixed in 4% PFA for 48 h. Tissue processing involved sequential dehydration through an ascending ethanol gradient, followed by xylene clearing and paraffin embedding. Serial sections of 5-μm thickness were obtained using a fully motorized rotary microtome (Leica RM2235, Wetzlar, Germany). Tissue sections were stained with hematoxylin and eosin (H&E) using standard protocols and examined under a bright-field microscope. A semi-quantitative scoring system was employed to assess pulmonary lesions: 0: Intact alveolar architecture, no evidence of inflammatory infiltration or vascular congestion; 1: Mild diffuse leukocyte infiltration in alveolar walls without structural alteration; 2: Moderate multifocal infiltration with 1–2× alveolar wall thickening; 3: Severe localized infiltration with 2–3× wall thickening in discrete regions; 4: Extensive consolidation (25–50% parenchymal involvement) with marked architectural distortion; 5: Diffuse consolidation (>50% involvement) with complete structural disruption.

Statistical Analysis

Experimental data were organized using Microsoft Excel and analyzed using GraphPad Prism (v9.4.1). Flow cytometry results were reported as cellular positivity rates, while other quantitative data were expressed as the mean ± standard error of measure (SEM). Parametric data were analyzed using one-way analysis of variance (ANOVA) followed by Tukey's post-hoc test, whereas non-parametric data were assesses using the Kruskal–Wallis test with Dunn's multiple comparisons test. Statistical significance was defined as $*p < 0.05$, $**p < 0.01$, $***p < 0.001$, $****p < 0.0001$, and ns (not significant).

Results

Design of RSV F DS2-Based NP Vaccine Platforms

Three distinct NP platforms—24-mer Fe, 60-mer LuS, and the 120-subunit I53-50 protein complex—were employed to present RSV DS2 antigens using structure-guided covalent conjugation and genetic fusion strategies (Figure 1A). For the Fe and LuS platforms, the ST-SC system enabled the site-specific display of DS2 trimers. In this design, the ST, a 16-residue peptide, was fused to the C-terminus of DS2 to preserve the pre-F conformation, while the SC, a 113-residue protein, was integrated into the

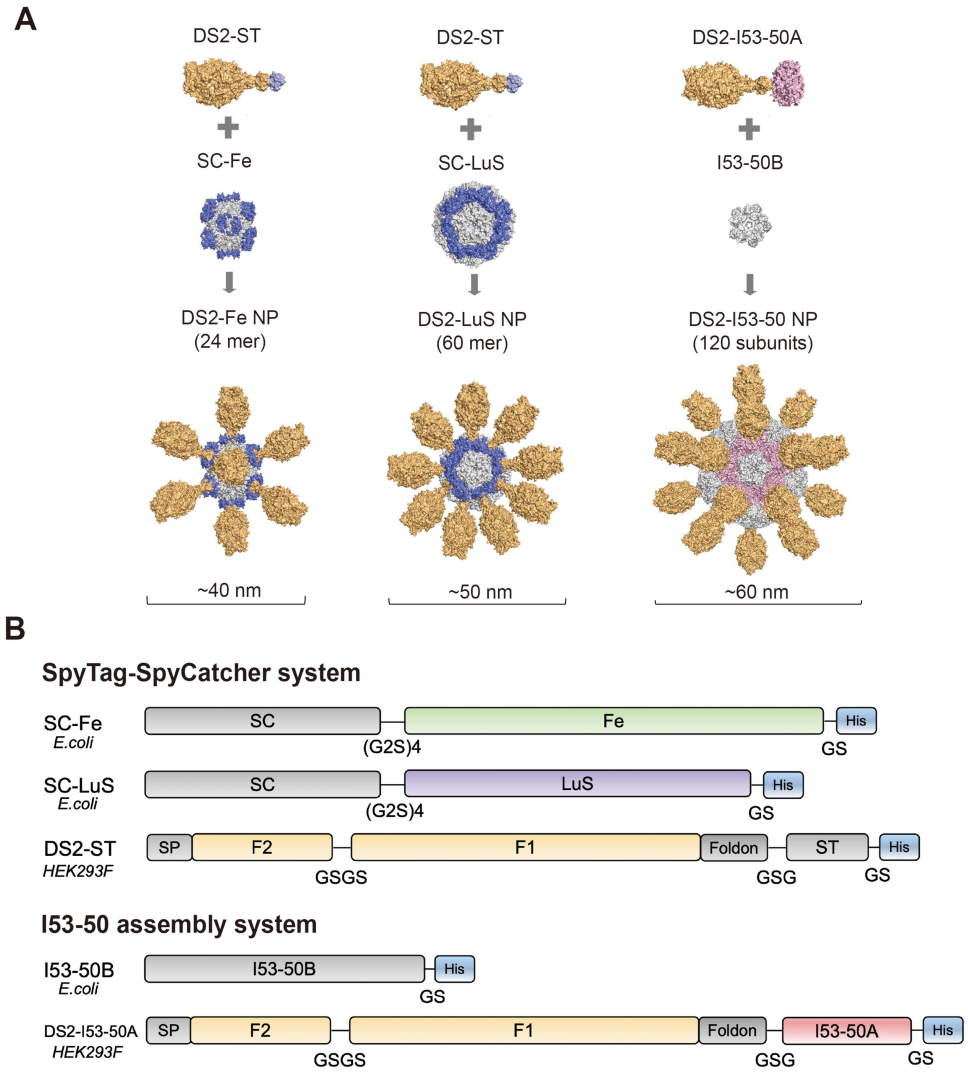

Figure 1 Design of three DS2-conjugated NP platforms. (**A**) Schematic illustration of self-assembly process for DS2-conjugated NPs via two distinct assembly approaches. Left two panels: DS2 proteins (gold) are site-specifically anchored to engineered Fe (gray) and LuS (gray) NPs through ST (light blue) and SC (dark blue)-mediated covalent conjugation. Right panel: DS2-fused I53-50A subunits (pink) co-assemble with I53-50B pentamers (gray) to form a stable icosahedral NP structure. (**B**) Modular plasmid architectures for targeted protein display across NP platforms, including the ST-SC conjugation system and the I53-50 self-assembly system. Molecular visualization in panel A was performed using PyMOL version 3.0.3 (https://pymol.org).

N-terminus of the NPs. The resulting SC-ST covalent conjugations produced two NP variants, designated as DS2-Fe and DS2-LuS, respectively (Figure 1B). The I53-50 platform, a computationally designed two-component protein complex, comprises 20 trimeric "A" components and 12 pentameric "B" components, forming a 120-subunit assembly.[15] DS2 was genetically fused to the trimeric component of I53-50 ("DS2-I53-50A") (Figure 1B), which spontaneously self-assembles with I53-50B through complementary electrostatic interfaces to form an icosahedral core (DS2-I53-50) (Figure 1A).

Preparation and Characterization of RSV F DS2-Conjugated NPs

The DS2-ST and DS2-I53-50A plasmids were successfully synthesized and transiently expressed in Expi293F cells (Figure 1B). Complementary NP component—SC-Fe (24-mer), SC-LuS (60-mer), I53-50A, and I53-50B—were expressed in an *Escherichia coli* system (Figure 1B). Target proteins were purified using sequential Ni-NTA chromatography and SEC. For ST-SC conjugation, SC-Fe or SC-LuS NPs were incubated with DS2-ST at a 1:2 molar ratio (NP to antigen), with optimized mixing ratios as detailed in Figure S1, yielding DS2-Fe or DS2-LuS NPs. Hierarchical assembly

https://doi.org/10.2147/IJN.S523340

of DS2-I53-50 or I53-50 NPs was achieved by mixing DS2-I53-50A or I53-50A and I53-50B subunits at a 1:1 molar ratio.

SDS-PAGE analysis confirmed successful conjugation, as evidenced by the appearance of higher molecular weight species in DS2-Fe and DS2-LuS conjugates, along with residual bands corresponding to the assembled components. The DS2-I53-50 conjugation was further validated through the simultaneous detection of both DS2-I53-50A and I53-50B components in the final mixture (Figure 2A). To elucidate the structural morphology of DS2-conjugated NPs, negative-staining EM analysis was employed. High-resolution EM imaging (Figure 2B) revealed that unconjugated NPs (SC-Fe, SC-LuS, and I53-50) formed monodisperse spherical nanostructures with uniform size distribution. Notably, DS2-conjugated NPs (DS2-Fe, DS2-LuS, and DS2-I53-50) exhibited distinct surface features, including increased roughness and protrusions, compared to the smoother surface of unconjugated NPs.

SEC analysis revealed that each unconjugated NPs eluted as a major peak at the expected volume (Figure 2C). In contrast, the three DS2-conjugated NPs exhibited earlier elution peaks, indicating successful assembly consistent with successful conjugation and the formation of larger assemblies (Figure 2C). DLS measurements (Figure 2D) further confirmed these findings, demonstrating a measurable increase in hydrodynamic diameter for DS2-conjugated NPs. Specifically, the hydrodynamic diameters of DS2-Fe, DS2-LuS, and DS2-I53-50 were determined to be 43.3 nm, 54.6 nm, and 64.8 nm, respectively, compared to their unconjugated counterparts (SC-Fe: 30.7 nm, SC-LuS: 41.7 nm, I53-50: 47.3 nm). Through this systematic approach, three distinct DS2-conjugated NPs with varying structural architectures and particle sizes were successfully prepared. Subsequent studies will focus on evaluating their antigenicity, immunogenicity, and potential as vaccine candidates.

In vitro Antigenic Profiling of RSV F DS2-Conjugated NPs

To characterize the structural integrity and immunogenic potential of the DS2-conjugated NPs (DS2-Fe, DS2-LuS, and DS2-I53-50), quantitative antigenicity assessments were performed using prefusion-specific neutralizing monoclonal antibodies D25 and AM14, which target antigenic sites Ø and V of RSV pre-F, respectively. These assessments were conducted using ELISA and SPR analysis. ELISA binding kinetics (Figure 3A) revealed that DS2-conjugated NPs displayed enhanced antibody binding affinity compared to DS2 trimer alone. SPR measurements (Figure 3B) further supported these findings, showing increased association kinetics for both D25 and AM14 antibodies. Quantitative analysis showed that the association rate constants (ka) (1/Ms) for D25 binding were 1.067×10^6 (DS2-Fe), 1.005×10^6 (DS2-LuS), and 1.394×10^6 (DS2-I53-50), yielding 9- to 12-fold improved affinity over DS2 trimers (1.138×10^5). Similarly, the AM14 binding kinetics demonstrated ka values of 3.172×10^6 (DS2-Fe), 3.800×10^6 (DS2-LuS), and 4.328×10^6 (DS2-I53-50), consistently representing 7- to 10-fold improvement over DS2 alone (4.384×10^5). Overall, these in vitro experiments demonstrate that DS2-conjugated NPs maintain the prefusion conformation of the DS2 trimer and exhibit superior antigenicity compared to DS2 trimers alone.

DS2-NP Vaccines Elicit Potent Humoral Immunity Response in BALB/c Mice

To evaluate the immunogenicity of DS2-based NP vaccines, BALB/c mice (n = 5 per group) received intramuscular injection in a prime-boost regimen (days 0 and 21) with 5 μg of soluble DS2 or equimolar doses of NP-conjugated formulations (DS2-Fe, DS2-LuS, and DS2-I53-50). The formulations were adjuvanted with 50 μg of aluminum hydroxide and 10 μg CpG. Control groups received PBS (mock) or empty NPs (SC-Fe, SC-LuS, I53-50) with adjuvant. Sera were collected on day 35 for immunological analysis (Figure 4A).

Quantitative assessment of humoral responses revealed that all DS2-containing formulations induced robust anti-DS2 IgG titers ($>3.2 \times 10^4$) following the booster immunization. Notably, DS2-I53-50 and DS2-LuS demonstrated significantly enhanced immunogenicity, with IgG antibody titers 2.9-fold and 2.3-fold higher, respectively, than soluble DS2 alone ($p < 0.05$) (Figure 4B). Isotype profiling indicated a Th2-biased response (IgG1/IgG2a > 1) across all groups, with DS2-NP formulations showing enhanced Th1 polarization. This was evidenced by significant reductions in IgG1/IgG2a ratios from 6.9 (DS2) to 3.4 (DS2-Fe), 3.0 (DS2-LuS), and 2.6 (DS2-I53-50) for the NP conjugates ($p < 0.05$). Furthermore, comparative analysis of IgG2a production revealed that DS2-I53-50 induced the highest IgG2a levels, followed by DS2-LuS and DS2-Fe, all of which surpassed the IgG2a levels elicited by soluble DS2 ($p < 0.05$)

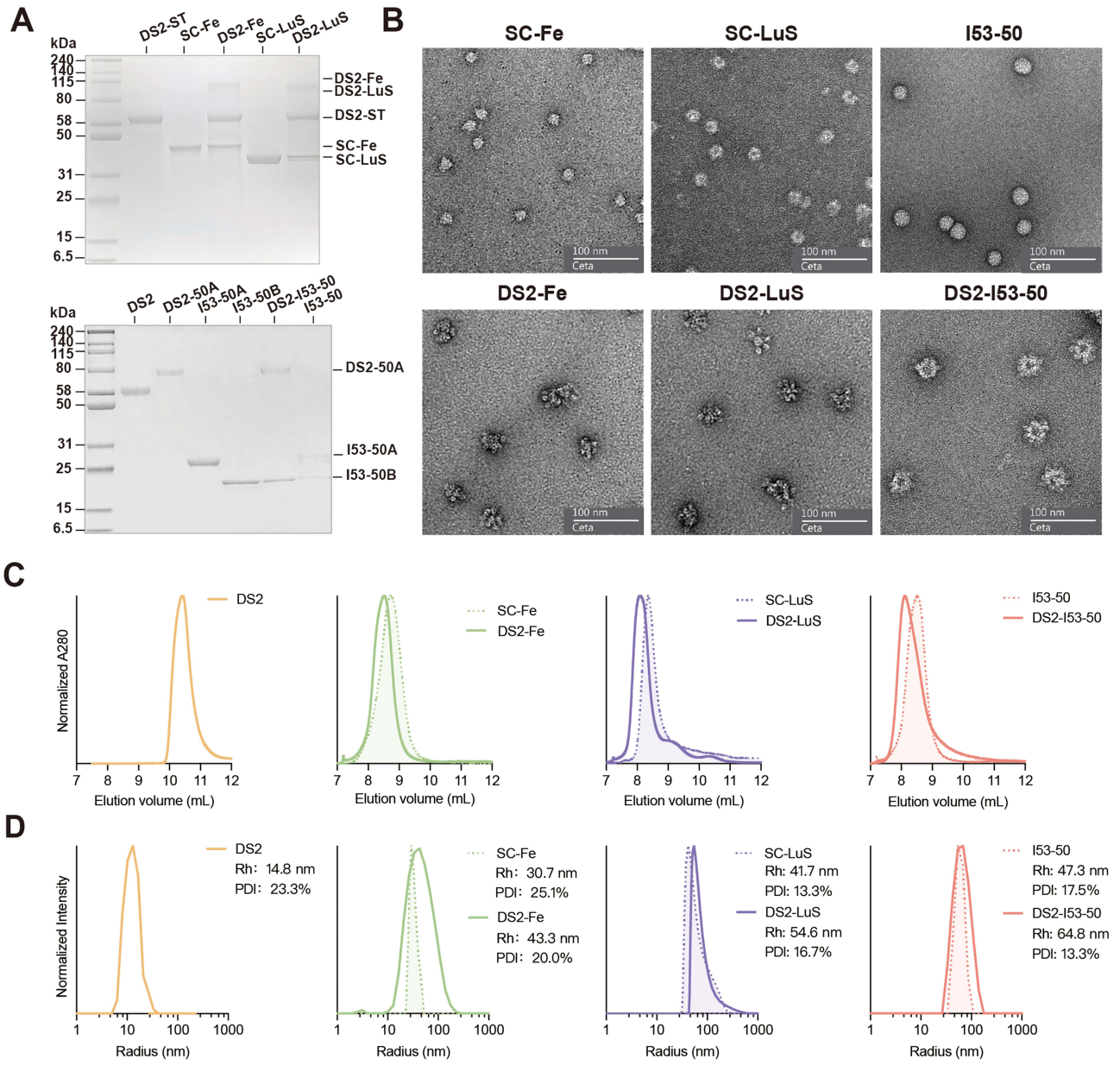

Figure 2 Biophysical characterization of three DS2-conjugated NPs. (**A**) Reducing SDS-PAGE analysis of various purified components and NPs. (**B**) Negative-staining electron micrographs showing both unconjugated NPs and DS2-conjugated NPs. (**C**) SEC profiles of DS2, DS2-conjugated NPs, and unconjugated NPs using the Superdex 200 Increase 10/300 GL column. Data represent a single replicate. (**D**) DLS analysis of DS2, DS2-conjugated NPs, and unconjugated NPs. Data show mean intensity values from three replicate measurements.

(Figure 4B). These findings highlight the superior capacity of NP platforms, particularly DS2-I53-50, to drive a more Th1-biased response, which is critical for effective viral neutralization and cellular immunity.[24]

Neutralization assays revealed that both DS2 and the three NP formulations induced robust cross-neutralizing antibodies against multiple RSV subtypes/genotypes strains. Quantitative analysis revealed that DS2 induced substantial neutralizing antibody titers, with geometric mean titers of 10,391 (LONG), 11,090 (ON1), 6,583 (18,537), and 9,545 (BA9) (Figure 4C). Among the tested formulations, DS2-I53-50 emerged as the most potent immunogen, demonstrating statistically significant enhancement in neutralizing capacity across all viral strains, with 1.7- to 2.4-fold higher neutralizing antibody titers compared to soluble DS2 ($p < 0.05$) (Figure 4C). In contrast, the DS2-Fe and DS2-LuS showed no significant enhancement in neutralizing capacity across all viral subtypes except for the RSV ON1 strain.

https://doi.org/10.2147/IJN.S523340

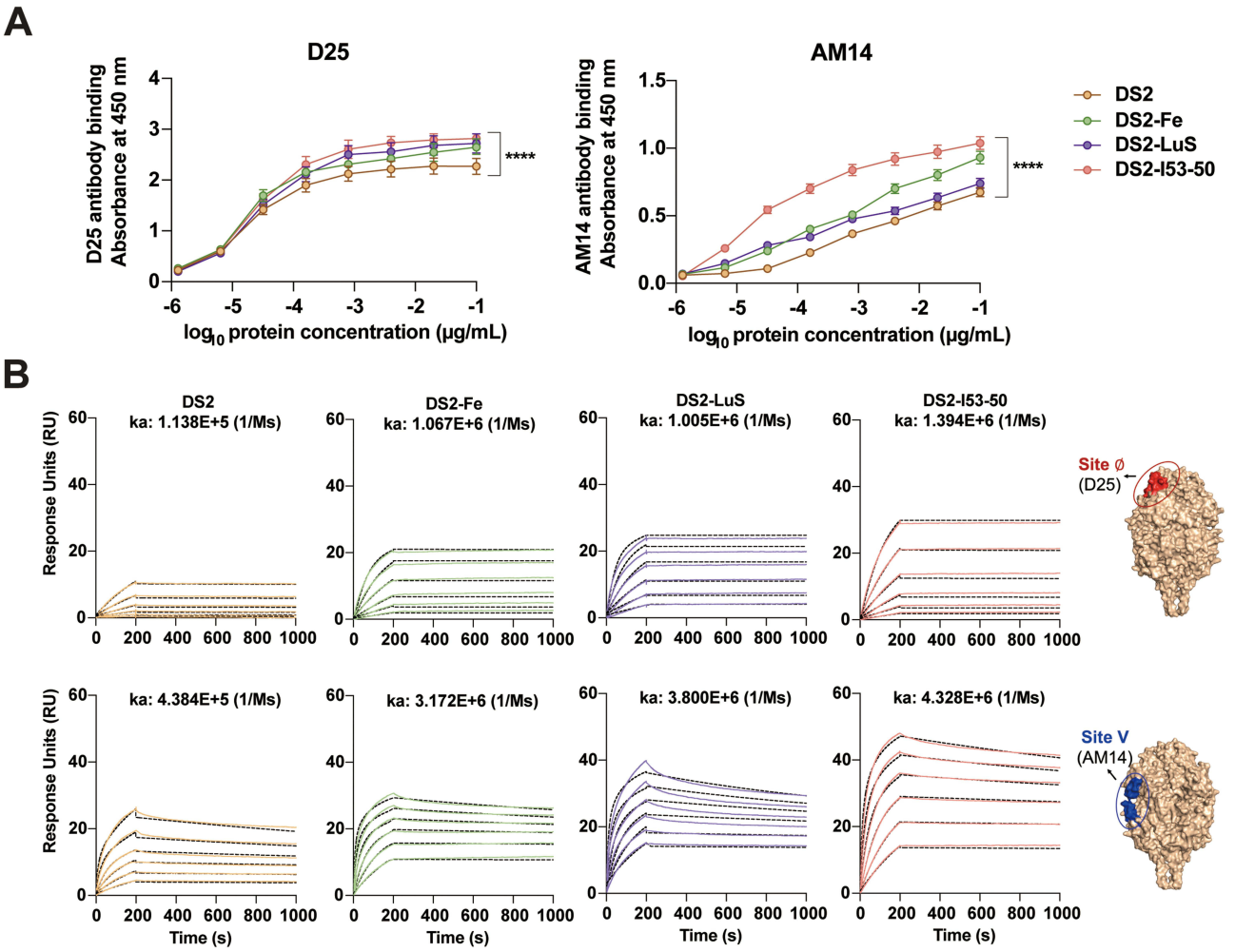

Figure 3 Antigenicity characterization of DS2 and DS2-conjugated NP immunogens. (**A**) Comparative binding kinetics of RSV PreF-specific monoclonal antibodies D25 (left panel) and AM14 (right panel) to DS2 and DS2-conjugated NPs, as determined via quantitative ELISA. Data represent mean and SEM from triplicate wells. (**B**) SPR response demonstrating real-time binding interactions between DS2-conjugated NPs and RSV PreF-specific antibodies. D25 and AM14 antibodies were immobilized on CM5 sensor chips, while antigen solutions (concentration range: 1.56–50 nM) were injected as analytes. Association rate constants (ka) were calculated from the sensorgram data. Molecular visualization of RSV Pre-F and its antigenic sites (Ø and V) was performed using PyMOL version 3.0.3 (https://pymol.org).

Cellular Immune Responses Induced by DS2-NP Vaccines in BALB/c Mice

NP vaccines enhance antigen uptake by dendritic cells (DCs) and macrophages, thereby promoting T follicular helper (Tfh) cell–B cell interactions.[25] To elucidate the cellular mechanisms underlying NP-mediated immune enhancement, flow cytometric analysis was performed on splenocytes from boost-immunized BALB/c mice, focusing on quantifying DCs, macrophages, GC B cells, and Tfh cell populations.

Flow cytometric analysis showed that all three DS2-conjugated NPs significantly exhibited higher DC levels compared to the DS2 group (Figure 5A, $p < 0.05$). Interestingly, only DS2-I53-50 showed a significant difference in macrophages compared to DS2 (Figure 5B), indicating its potential role in modulating macrophage activity. For Tfh and GC B cells, DS2-Fe and DS2-LuS showed numerical increases compared to the DS2 group, but these differences were not statistically significant. In contrast, DS2-I53-50 induced significantly elevated Tfh cell and GC B cell populations (Figure 5C and D; Figure S2, $p < 0.05$), suggesting enhanced GC formation and potentially improved humoral immunity.

Detailed analysis of T cell memory subsets revealed that both DS2-I53-50 and DS2-LuS significantly expanded $CD4^+$ central memory T cell (Tcm) and effector memory T cell (Tem) populations compared to the DS2 group (Figure 5E and F, $p < 0.05$). This finding suggests that NP conjugation might not only enhance antigen presentation but also promote the development of long-lasting cellular immunity through the generation of memory T cell populations. However,

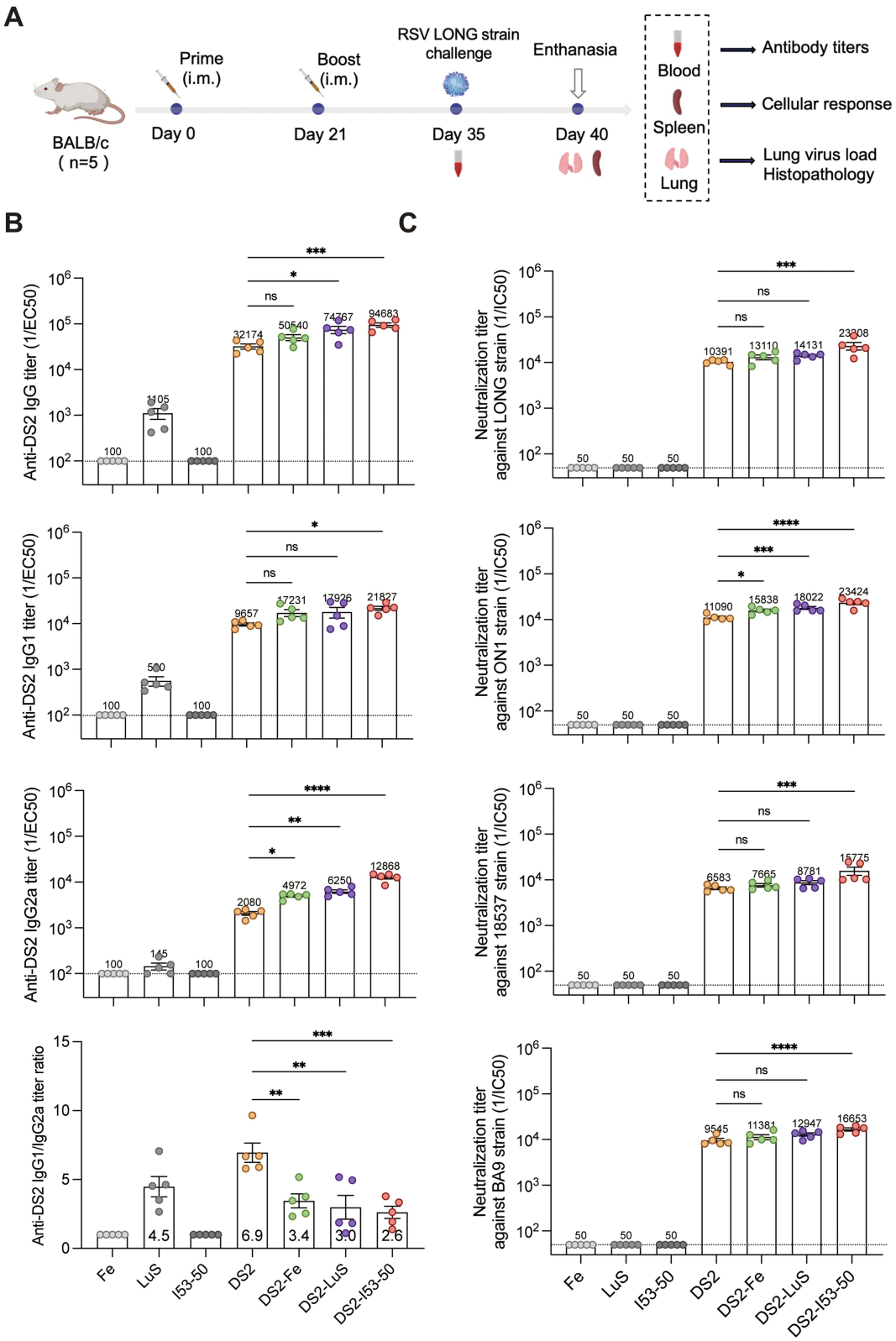

Figure 4 Humoral immune responses elicited by DS2-NP vaccines in BALB/c mice. (**A**) Schematic representation of the immunization-challenge protocol. BALB/c mice (n = 5 per group) were immunized via intramuscular injection at days 0 and 21, challenged with RSV-LONG strain at day 35, and euthanized at day 40 for tissue collection and analysis. (**B**) Quantification of DS2-specific IgG antibody titers in day 35 serum samples via ELISA. Titers were determined through four-parameter logistic regression analysis of serial dilutions and expressed as reciprocal EC_{50} values. The dashed line indicates the seropositivity threshold (100). (**C**) Neutralizing antibody titers of each vaccine group were assessed using a plaque reduction neutralization test and are represented as IC_{50} values. The dashed line indicates the seropositivity threshold (50). Statistical comparisons between the DS2 and DS2-NP groups was determined using the Mann–Whitney *U*-test. Data present mean ± SEM in panels B–C, with mean values for each group indicated at the corresponding data points. Statistical significance is denoted as follows: **p* < 0.05; ***p* < 0.01; ****p* < 0.001; *****p* < 0.0001; ns, not significant.

https://doi.org/10.2147/IJN.S523340

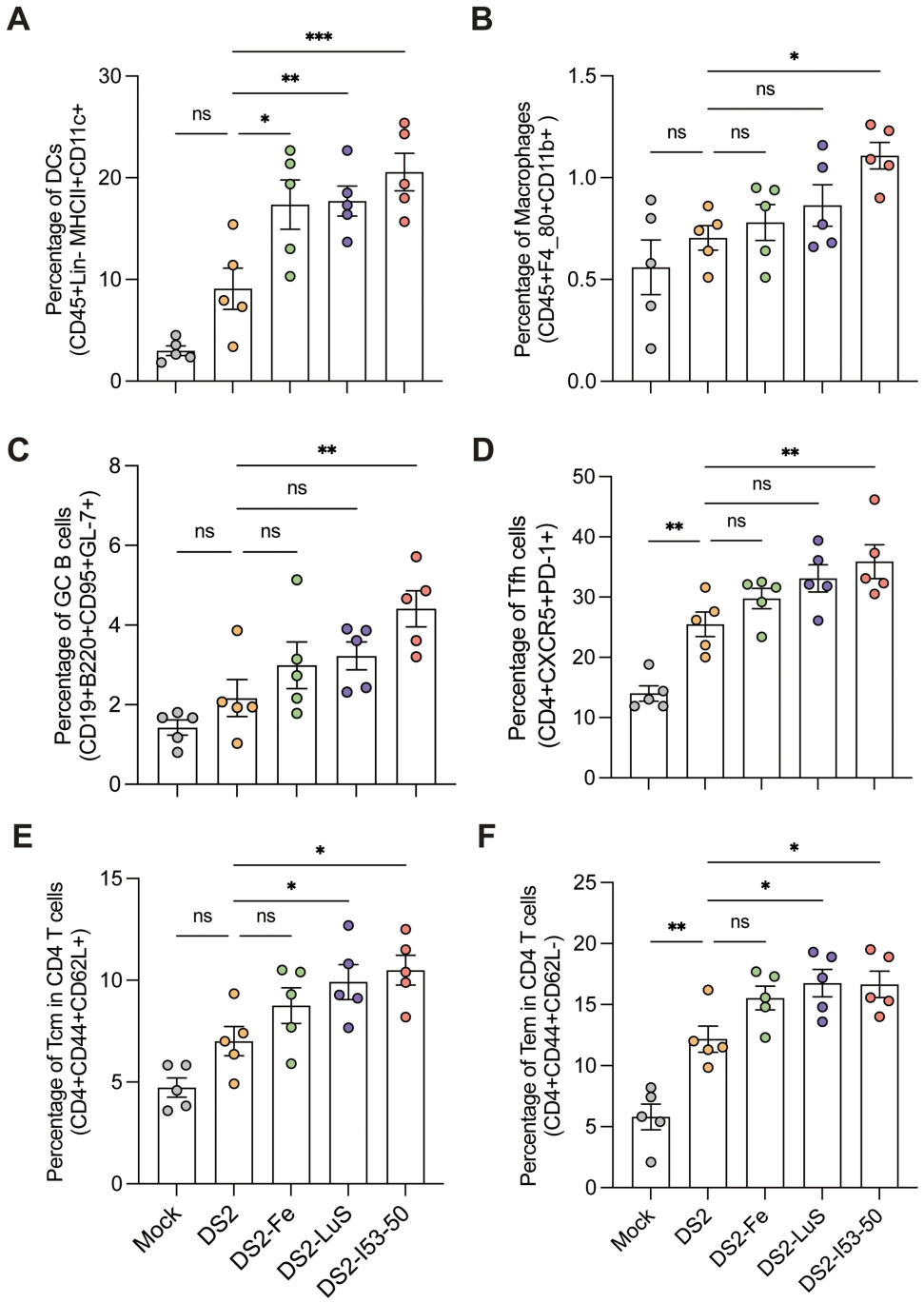

Figure 5 Cellular responses in NP-vaccinated BALB/c mice. (**A–F**) Percentages of DCs ($CD45^+Lin\text{-}MHCII^+CD11c^+$), macrophages ($CD45^+F4/80^+CD11b^+$), GC B cells ($CD19^+B220^+CD95^+GL\text{-}7^+$), Tfh cells ($CD4^+CXCR5^+PD\text{-}1^+$), Tcm cells ($CD4^+CD44^+CD62L^+$), and Tem cells ($CD4^+CD44^+CD62L^-$) in spleen cell suspensions were quantified via flow cytometry (n = 5). Data are presented as mean ± SEM. Statistical significance was determined using one-way ANOVA followed by Tukey's post-hoc test. Significance levels are denoted as follows: $^*p < 0.05$; $^{**}p < 0.01$; $^{***}p < 0.001$; ns, not significant.

intracellular cytokine staining of splenocytes from DS2-NP-immunized mice revealed no significant increase in cytokine-producing immune cells compared to the DS2 group (Figure S3).

DS2-NP Vaccines Protect Against RSV Infection in BALB/c Mice

To evaluate the protective efficacy of DS2 and DS2-NPs vaccines against RSV infection, BALB/c mice were intranasally challenged with 6×10^5 PFUs of RSV LONG strain 2 weeks post-boost vaccination and subsequently euthanized 5 d post-

challenge (Figure 5A). Analysis of body weight changes revealed distinct patterns among the experimental groups. Notably, control groups (PBS, SC-Fe, SC-LuS, and I53-50) manifested significant weight reduction, with all groups except I53-50 experiencing a decline below 80% of their initial body weight by day 5 post-challenge. In contrast, all immunized groups initiated body weight recovery by day 2 post-challenge, with the DS2-I53-50 group exhibiting the most rapid recovery, followed by the DS-Fe and DS2-LuS groups (Figure 6A).

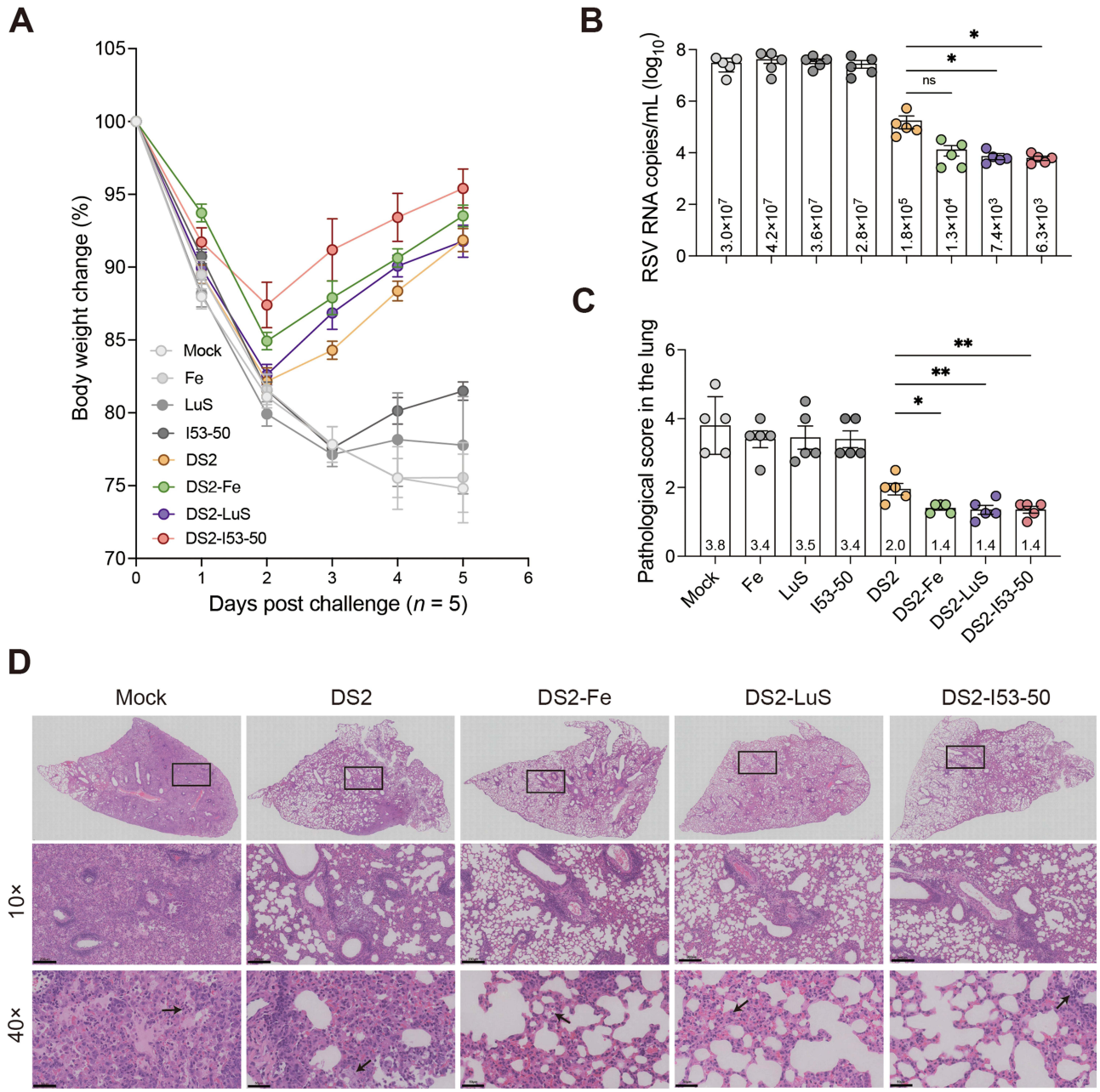

Figure 6 Evaluation of DS2 NP vaccine efficacy against RSV LONG virus challenge in BALB/c mice. (**A**) Body weight changes (expressed as percentage of initial weight) in mice following RSV challenge. Data represent mean ± SEM. (**B**) Quantification of pulmonary viral load (RSV N gene copies) across experimental groups. Data are shown as mean ± SEM, with group means annotated below the plot. (**C**) Pathological injury scores in lung tissues post-challenge. Data shown as mean ± SEM, with group means annotated below the plot. (**D**) Representative histopathological images (H&E staining) analysis of lung tissue from individual mice in mock, DS2, and DS2-NPs groups. Images were acquired at 10× and 40× magnification, with scale bars in the lower left corner representing 200 μm and 50 μm, respectively. Black arrows indicate the presence of neutrophils and lymphocytes within alveolar lumina. Statistical analysis was conducted using one-way ANOVA followed by Tukey's post-hoc test. Significance levels are indicated as: *$p < 0.05$; **$p < 0.01$; ns, not significant.

https://doi.org/10.2147/IJN.S523340

Quantitative RT-PCR analysis of lung tissues revealed high RSV RNA levels (> 2.8×10^7 copies/mL) across all control groups, confirming robust viral replication (Figure 6B). In contrast, vaccinated mice exhibited significantly reduced viral RNA levels. Compared to the PBS control, DS2 alone reduced viral loads by 2.2 log, while NP formulations showed enhanced efficacy: DS2-Fe reduced viral loads by 3.4 log, DS2-LuS by 3.6 log, and DS2-I53-50 demonstrated the greatest reduction, with viral loads decreased by 3.7 log (Figure 6B). These results indicated that the NP formulations effectively inhibited RSV replication by inducing robust immune responses.

Histopathological analysis of lung tissues revealed distinct pathological changes following RSV challenge. Control groups exhibited severe lung damage, characterized by alveolar septal thickening, inflammatory cell infiltration, and peribronchial and peritracheal inflammation (Figure 6D). In contrast, vaccinated groups showed significantly attenuated pathology. DS2-immunized mice showed localized inflammation, while DS2-NP-treated animals demonstrated minimal pathological alterations (Figure 6D). Quantitative analysis of lung pathology scores further supported these observations, with DS2-immunized mice showing a moderate score of 2.0, while DS2-NP-vaccinated mice exhibited the lowest score of 1.4 (Figure 6C). The superior efficacy of DS2-NP formulations in reducing weight loss, mitigating lung damage, and lowering viral loads underscores their enhanced protective efficacy and highlights their potential as a promising strategy for RSV vaccine development.

Discussion

NP-based immunogens can mimic the geometric patterns of viral pathogens, promote efficient B cell receptor (BCR) crosslinking, and induce potent neutralizing antibodies responses, making them promising platforms for RSV vaccine development.[26,27] To evaluate the immunogenic potential of different NP scaffolds for displaying a stabilized RSV prefusion F antigen (DS2), we engineered and characterized three DS2-NP vaccines: DS2-Fe, DS2-LuS, and DS2-I53-50. DS2-Fe and DS2-LuS were assembled using the ST–SC conjugation system to link DS2 to the NP scaffold, while DS2-I53-50 was produced via direct genetic fusion of DS2 to the I53-50A subunit, which subsequently self-assembles with the complementary I53-50B component. Biophysical analyses confirmed that all three NPs were successfully assembled through optimized expression and conjugation methods.[15,22]

In this study, we focused on the DS2 antigen, which preserves the structural architecture of the prefusion conformation of RSV F protein and contains critical neutralizing epitopes, including antigenic sites Ø and V.[6] Antigen–antibody kinetic analyses demonstrated that all three DS2-NPs exhibited enhanced antigenicity in vitro compared to soluble DS2, as evidenced by increased binding affinities to prefusion-specific monoclonal antibodies (D25 and AM14) and SPR kinetics. Notably, AM14[6]—which targets a quaternary epitope unique to the prefusion trimer—showed particularly enhanced binding, suggesting that NP conjugation may help stabilize DS2 in its prefusion conformation and improve epitope accessibility critical for optimal immunogenicity.

Neutralizing antibodies are well-established correlate of protection against RSV infection.[28,29] In vivo, all three DS2-NPs elicited significantly higher titers of neutralizing antibodies against prototype (RSV Long and 18537) and wild strains (ON1 and BA9) compared to soluble DS2. Among them, DS2-I53-50 induced the highest antibody titers and robust germinal center B cells (GCBs) and T follicular helper (Tfh) cell responses. One potential explanation for this enhanced immunogenicity is the relatively larger hydrodynamic diameter (~64.8 nm) of DS2-I53-50, which falls within the 50–100 nm size range previously associated with optimal immune activation.[30–32] NPs of this size are more efficiently retained by follicular dendritic cells and are more likely to undergo complement-mediated opsonization, thereby enhancing antigen presentation and subsequent humoral responses.[30–32] Another factor may be the superior conjugation efficiency and particle uniformity of DS2-I53-50. While the ST–SC conjugation system offers versatility, conjugation efficiency can be affected by various factors.[23] In our study, DS2-Fe and DS2-LuS exhibited lower conjugation efficiency and less uniform antigen distribution on particle surfaces, as indicated by SDS-PAGE and electron microscopy analyses. These differences in particle quality may contribute to their relatively reduced immunogenicity compared to DS2-I53-50. Conversely, direct genetic fusion of antigens to NP subunits, as implemented with DS-Cav1-I53-50, gB-I53-50 and DS-Cav1-Fe, may enhance antigen display efficiency and particle uniformity.[19,20,33] These findings underscore the critical role of NP design, purification, and particle quality in shaping immune responses.

Beyond humoral immunity, effective RSV vaccines must also elicit durable and balanced cellular immunity.[34] Central and effector memory T cell populations (Tcm and Tem) are essential for rapid recall responses upon viral re-exposure, contributing to viral clearance and long-term protection.[35,36] In our study, both DS2-I53-50 and DS2-LuS significantly expanded $CD4^+$ Tcm and Tem populations compared to soluble DS2, indicating their potential to elicit durable cellular immunity. Furthermore, DS2-NPs induced a more balanced Th1/Th2 response, as reflected by lower IgG1/IgG2a ratios, compared to soluble DS2. A Th1-biased response is critical for viral clearance and for minimizing the risk of vaccine-enhanced respiratory disease, a concern previously highlighted by the FI-RSV vaccine.[2,34,37] Animal challenge studies further demonstrated that all three DS2-NPs conferred robust protection against RSV infection, significantly reducing viral loads and mitigating lung pathology. These findings corroborate and expand on previous preclinical studies supporting the efficacy of RSV NP vaccines.[38,39] The enhanced protection observed for DS2-NPs compared to soluble DS2 likely stems from stronger humoral and cellular immune responses, as well as improved antigen presentation and tissue retention mediated by NP platforms. Together, these results support DS2-based NPs as a promising RSV vaccine strategy capable of delivering broad protection with a favorable safety and immunogenicity profile.

Despite these promising results, several important challenges remain to be addressed. First, although DS2-Fe and DS2-LuS demonstrated improved immunogenicity compared to soluble DS2, efforts to enhance conjugation efficiency and particle homogeneity to improve particle quality should be prioritized. This may include exploring direct fusion approaches or alternative site-specific conjugation methods. Second, while initial data suggest the potential for durable memory responses, longitudinal studies are needed to confirm the longevity of memory B or T cell populations. third, dose–response experiments are required to identify the minimum protective dose and inform dose-sparing strategies for clinical translation. Finally, the effects of various adjuvants on the immunogenicity and safety of DS2-NPs remain unexplored and may present opportunities for further enhancement of immune responses.

Conclusion

In this study, we developed and characterized three structurally distinct DS2-conjugated NPs vaccine candidates—DS2-Fe, DS2-LuS, and DS2-I53-50. All three showed improved immunogenicity and protective efficacy over soluble DS2, with notable differences between platforms. These results emphasize the need to optimize nanoparticle design, antigen conjugation, and particle quality to advance RSV NP vaccine development. Our findings offer valuable insights for the rational design of future NP vaccines and support broader efforts in infectious disease prevention.

Acknowledgments

This work was supported by the National Key Research and Development Program of China (No. 2024YFC2310401), Beijing Natural Science Foundation of China (No. L222122).

Disclosure

The authors report no conflicts of interest in this work.

References

1. Li Y, Wang X, Blau DM, et al. Global, regional, and national disease burden estimates of acute lower respiratory infections due to respiratory syncytial virus in children younger than 5 years in 2019: a systematic analysis. *Lancet Lond Engl*. 2022;399(10340):2047–2064. doi:10.1016/S0140-6736(22)00478-0
2. Kelleher K, Subramaniam N, Drysdale SB. The recent landscape of RSV vaccine research. *Ther Adv Vaccines Immunother*. 2025;13:25151355241310601. doi:10.1177/25151355241310601
3. Mullard A. FDA approves mRNA-based RSV vaccine. *Nat Rev Drug Discov*. 2024;23(7):487. doi:10.1038/d41573-024-00095-3
4. Anastassopoulou C, Medić S, Ferous S, Boufidou F, Development TA. Current Status, and Remaining Challenges for Respiratory Syncytial Virus Vaccines. *Vaccines*. 2025;13(2):97. doi:10.3390/vaccines13020097
5. McLellan JS, Chen M, Leung S, et al. Structure of RSV fusion glycoprotein trimer bound to a prefusion-specific neutralizing antibody. *Science*. 2013;340(6136):1113–1117. doi:10.1126/science.1234914
6. Gilman MSA, Moin SM, Mas V, et al. Characterization of a Prefusion-Specific Antibody That Recognizes a Quaternary, Cleavage-Dependent Epitope on the RSV Fusion Glycoprotein. *PLoS Pathog*. 2015;11(7):e1005035. doi:10.1371/journal.ppat.1005035
7. McLellan JS, Chen M, Joyce MG, et al. Structure-based design of a fusion glycoprotein vaccine for respiratory syncytial virus. *Science*. 2013;342(6158):592–598. doi:10.1126/science.1243283

8. Joyce MG, Zhang B, Ou L, et al. Iterative structure-based improvement of a fusion-glycoprotein vaccine against RSV. *Nat Struct Mol Biol*. 2016;23(9):811–820. doi:10.1038/nsmb.3267
9. Krarup A, Truan D, Furmanova-Hollenstein P, et al. A highly stable prefusion RSV F vaccine derived from structural analysis of the fusion mechanism. *Nat Commun*. 2015;6:8143. doi:10.1038/ncomms9143
10. Liang Y, Shao S, Li XY, et al. Mutating a flexible region of the RSV F protein can stabilize the prefusion conformation. *Science*. 2024;385(6716):1484–1491. doi:10.1126/science.adp2362
11. Gao X, Wang X, Li S, Saif Ur Rahman M, Xu S, Liu Y. Nanovaccines for Advancing Long-Lasting Immunity against Infectious Diseases. *ACS Nano*. 2023;17(24):24514–24538. doi:10.1021/acsnano.3c07741
12. Liu S, Hu M, Liu X, et al. Nanoparticles and Antiviral Vaccines. *Vaccines*. 2024;12(1):30. doi:10.3390/vaccines12010030
13. Ols S, Lenart K, Arcoverde Cerveira R, et al. Multivalent antigen display on nanoparticle immunogens increases B cell clonotype diversity and neutralization breadth to pneumoviruses. *Immunity*. 2023;56(10):2425–2441.e14. doi:10.1016/j.immuni.2023.08.011
14. Nguyen B, Tolia NH. Protein-based antigen presentation platforms for nanoparticle vaccines. *NPJ Vaccines*. 2021;6(1):70. doi:10.1038/s41541-021-00330-7
15. Bale JB, Gonen S, Liu Y, et al. Accurate design of megadalton-scale two-component icosahedral protein complexes. *Science*. 2016;353(6297):389–394. doi:10.1126/science.aaf8818
16. Boyoglu-Barnum S, Ellis D, Gillespie RA, et al. Quadrivalent influenza nanoparticle vaccines induce broad protection. *Nature*. 2021;592(7855):623–628. doi:10.1038/s41586-021-03365-x
17. Jardine JG, Kulp DW, Havenar-Daughton C, et al. HIV-1 broadly neutralizing antibody precursor B cells revealed by germline-targeting immunogen. *Science*. 2016;351(6280):1458–1463. doi:10.1126/science.aad9195
18. Ma X, Zou F, Yu F, et al. Nanoparticle Vaccines Based on the Receptor Binding Domain (RBD) and Heptad Repeat (HR) of SARS-CoV-2 Elicit Robust Protective Immune Responses. *Immunity*. 2020;53(6):1315–1330.e9. doi:10.1016/j.immuni.2020.11.015
19. Marcandalli J, Fiala B, Ols S, et al. Induction of Potent Neutralizing Antibody Responses by a Designed Protein Nanoparticle Vaccine for Respiratory Syncytial Virus. *Cell*. 2019;176(6):1420–1431.e17. doi:10.1016/j.cell.2019.01.046
20. Sun C, Kang YF, Fang XY, et al. A gB nanoparticle vaccine elicits a protective neutralizing antibody response against EBV. *Cell Host Microbe*. 2023;31(11). doi:10.1016/j.chom.2023.09.011
21. Keeble AH, Turkki P, Stokes S, et al. Approaching infinite affinity through engineering of peptide–protein interaction. *Proc Natl Acad Sci*. 2019;116(52):26523–26533. doi:10.1073/pnas.1909653116
22. Kang YF, Sun C, Zhuang Z, et al. Rapid Development of SARS-CoV-2 Spike Protein Receptor-Binding Domain Self-Assembled Nanoparticle Vaccine Candidates. *ACS Nano*. 2021;15(2):2738–2752. doi:10.1021/acsnano.0c08379
23. Li Q, Zhang J, Deng Q, et al. A Divalent Chikungunya and Zika Nanovaccine with Thermostable Self-Assembly Multivalent Scaffold LS-SUMO. *Adv Healthc Mater*. 2024:e2303619. doi:10.1002/adhm.202303619.
24. van der Fits L, Bolder R, Heemskerk-van der Meer M, et al. Adenovector 26 encoded prefusion conformation stabilized RSV-F protein induces long-lasting Th1-biased immunity in neonatal mice. *NPJ Vaccines*. 2020;5(1):49. doi:10.1038/s41541-020-0200-y
25. Kelly HG, Tan HX, Juno JA, et al. Self-assembling influenza nanoparticle vaccines drive extended germinal center activity and memory B cell maturation. *JCI Insight*. 2020;5(10):e136653. doi:10.1172/jci.insight.136653
26. Bachmann MF, Jennings GT. Vaccine delivery: a matter of size, geometry, kinetics and molecular patterns. *Nat Rev Immunol*. 2010;10(11):787–796. doi:10.1038/nri2868
27. Chackerian B, Durfee MR, Schiller JT. Virus-Like Display of a Neo-Self Antigen Reverses B Cell Anergy in a B Cell Receptor Transgenic Mouse Model. *J Immunol*. 2008;180(9):5816–5825. doi:10.4049/jimmunol.180.9.5816
28. Gruell H, Vanshylla K, Weber T, Barnes CO, Kreer C, Klein F. Antibody-mediated neutralization of SARS-CoV-2. *Immunity*. 2022;55(6):925–944. doi:10.1016/j.immuni.2022.05.005
29. Soto JA, Stephens LM, Waldstein KA, Canedo-Marroquín G, Varga SM, Kalergis AM. Current Insights in the Development of Efficacious Vaccines Against RSV. *Front Immunol*. 2020;11:1507. doi:10.3389/fimmu.2020.01507
30. Irvine DJ, Read BJ. Shaping humoral immunity to vaccines through antigen-displaying nanoparticles. *Curr Opin Immunol*. 2020;65:1–6. doi:10.1016/j.coi.2020.01.007
31. Irvine DJ, Hanson MC, Rakhra K, Tokatlian T. Synthetic Nanoparticles for Vaccines and Immunotherapy. *Chem Rev*. 2015;115(19):11109. doi:10.1021/acs.chemrev.5b00109
32. Zhang YN, Lazarovits J, Poon W, et al. Nanoparticle Size Influences Antigen Retention and Presentation in Lymph Node Follicles for Humoral Immunity. *Nano Lett*. 2019;19(10):7226–7235. doi:10.1021/acs.nanolett.9b02834
33. Swanson KA, Rainho-Tomko JN, Williams ZP, et al. A respiratory syncytial virus (RSV) F protein nanoparticle vaccine focuses antibody responses to a conserved neutralization domain. *Sci Immunol*. 2020;5(47):eaba6466. doi:10.1126/sciimmunol.aba6466
34. Higgins D, Trujillo C, Keech C. Advances in RSV vaccine research and development – a global agenda. *Vaccine*. 2016;34(26):2870–2875. doi:10.1016/j.vaccine.2016.03.109
35. Jameson SC, Masopust D. Understanding subset diversity in T cell memory. *Immunity*. 2018;48(2):214. doi:10.1016/j.immuni.2018.02.010
36. Sallusto F, Lanzavecchia A, Araki K, Ahmed R. From vaccines to memory and back. *Immunity*. 2010;33(4):451–463. doi:10.1016/j.immuni.2010.10.008
37. Eichinger KM, Kosanovich JL, Gidwani SV, et al. Prefusion RSV F Immunization Elicits Th2-Mediated Lung Pathology in Mice When Formulated With a Th2 (but Not a Th1/Th2-Balanced) Adjuvant Despite Complete Viral Protection. *Front Immunol*. 2020;11:1673. doi:10.3389/fimmu.2020.01673
38. Stephens L, Ross KA, McLellan JS, Narasimhan B, Varga SM. Robust efficacy and long-lasting humoral immunity induced by a respiratory syncytial virus prefusion F-based nanoparticle vaccine in genetically diverse animal models. *J Immunol*. 2022;208(1_Supplement):64. doi:10.4049/jimmunol.208.Supp.64.14
39. Voorzaat R, Cox F, van Overveld D, et al. Design and Preclinical Evaluation of a Nanoparticle Vaccine against Respiratory Syncytial Virus Based on the Attachment Protein G. *Vaccines*. 2024;12(3):294. doi:10.3390/vaccines12030294